University of Huddersfield Repository

Reading, M. A., Van den Berg, Jakob, Zalm, P. C., Armour, D. G., Bailey, Paul, Noakes, T. C. Q., Parisini, A., Conard, T. and De Gendt, S.

High resolution medium energy ion scattering analysis for the quantitative depth profiling of ultrathin high-k layers

Original Citation

This version is available at http://eprints.hud.ac.uk/12263/

http://eprints.hud.ac.uk/

High resolution medium energy ion scattering analysis for the quantitative depth profiling of ultrathin high-*k* layers

M. A. Reading,[a)] J. A. van den Berg, P. C. Zalm, and D. G. Armour
Institute for Materials Research, University of Salford, Salford M5 4WT, United Kingdom

P. Bailey and T. C. Q. Noakes
STFC Daresbury Laboratory, Daresbury WA4 4AD, United Kingdom

A. Parisini
CNR-IMM Sezione Bologna, Via Gobetti, 40129 Bologna, Italy

T. Conard and S. De Gendt
IMEC, Kapeldreef 75, 3001 Leuven, Belgium

Ultrathin high-*k* layers such as hafnium oxide (HfO_2) in combination with a subnanometer SiO_2 or Hf silicate have emerged as Si compatible gate dielectric materials. Medium energy ion scattering (MEIS) analysis has been carried out on a range of such metal oxide chemical vapor deposition grown HfO_2/SiO_2 and $HfSiO_x(60\%\,Hf)/SiO_2$ gate oxide films of thickness between 1 and 2 nm on Si(100), before and after decoupled plasma nitridation (DPN). The ability of MEIS in combination with energy spectrum simulation to provide quantitative layer information with subnanometer resolution is illustrated and the effect of the DPN process is shown. Excellent agreement on the deduced layer structures and atomic composition with the as grown layer parameters, as well as with those obtained from cross section electron microscopy and other studies, is demonstrated. MEIS analysis of a high-*k*, metal gate $TiN/Al_2O_3/HfO_2/SiO_2/Si$ stack shows the interdiffusion, after thermal treatment, of Hf and Al from the caplayer, inserted to modify the metal gate workfunction. © *2010 American Vacuum Society*. [DOI: 10.1116/1.3248264]

I. INTRODUCTION

In the past decade or so, an intensive R&D effort has been made to identify high-*k* gate dielectrics with suitable chemical, structural, and electrical characteristics to replace SiO_2 in complementary metal oxide semiconductor device manufacture. This was driven by the need to overcome prohibitive leakage problems in SiO_2 posed by electron tunneling as scaling of gate oxide thicknesses approached 1 nm.[1] Of the range of binary oxides investigated, HfO_2 and silicates have emerged as promising gate dielectric materials and, in fact, HfO_2 dielectrics in combination with a subnanometer SiO_2 and metal gate have been introduced in the 45 nm generation device processing.[2] Also nitridation is often applied to improve the oxide characteristics, such as, e.g., thermal stability.[3,4]

The accurate structural and compositional characterizations of these layers, though vital as it enables an understanding of their properties and the ability to tailor these, also pose a severe challenge that pushes the capability of analytical techniques to the limit. One activity within the analytical network for micro- and nanoanalysis (ANNA) project[5] is the optimization of a range of high depth resolution analytical techniques for this task. Medium energy ion scattering (MEIS), as one of the techniques investigated, is in principle capable of giving quantitative information on the structure and composition of shallow layers with subnanometer depth resolution near the surface[6–8] and has for that reason been applied to the characterization of thin high-*k* layers and aspects of their growth by a number of groups.[6,9–15] However, the realization of this ability of MEIS especially for ultrathin, multicomponent films is increasingly contingent on the availability of a suitable simulation model that takes into account all collisional effects that occur during the process of penetration, scattering, and emergence including, e.g., composition dependent stopping, straggling, cross section correction, and projectile neutralization.

In order to evaluate and demonstrate this capability of MEIS, the technique has been applied to a series of very thin, Hf based oxide and silicate films grown by metal oxide chemical vapor deposition (MOCVD) at IMEC, which contain a systematic change in variable (details given below). The extraction of the compositional and structural layer information is based on the application of a simulation program, written as a macro within the IGOR[©] graphing package[16] and developed at Daresbury Laboratory,[17] which will be briefly described. Aspects of the quantification of the MEIS yield included in the model will be first discussed. The excellent agreement on the deduced layer structures and atomic composition with the as grown layer parameters, as well as with those obtained from parallel cross section electron microscopy (XTEM) and other studies carried out within the ANNA project, will be demonstrated. Finally, a MEIS analysis of a complex, ~7 nm wide, high-*k* metal gate stack of the following structure will be presented: $TiN/Al_2O_3/HfO_2/SiO_2/Si$. Not only does the technique re-

[a)]Electronic mail: m.a.reading@pgr.salford.ac.uk

TABLE I. Structure of the samples as grown and treated. DPN refers to decoupled plasma nitriding.

Sample No.	Substrate	First layer	Process	Second layer	Process
D02	Si	1 nm SiO_2			
D03	Si	1 nm SiO_2	DPN		
D05	Si	1 nm SiO_2		2 nm HfO_2	
D06	Si	1 nm SiO_2		2 nm HfO_2	DPN
D07	Si	1 nm SiO_2		2 nm $HfSiO_2$	
D08	Si	1 nm SiO_2		2 nm $HfSiO_2$	DPN
D09	Si	1 nm SiO_2	DPN	2 nm $HfSiO_2$	DPN

produce the as grown film parameters but it also indicates the diffusion, after thermal treatment at 1025 °C, of Hf into the Al caplayer and of Al into the high-*k* layer.[18]

II. EXPERIMENT

Unpatterned Si(100) wafers were prepared using an IMEC clean,[19] leading to the growth of a 1 nm SiO_2 layer on the Si surface, followed by planar deposition of a nominally 2 nm HfO_2 or $HfSiO_x$ (60% Hf) layer on top of the SiO_2 by MOCVD, all performed at IMEC. Some samples underwent decoupled plasma nitridation (DPN) at 800 °C.[20,21] In addition, reference samples without the Hf layer were produced with and without DPN. Full details of the layer structures are given in Table I. Samples were analyzed in ultrahigh vacuum using the MEIS facility at Daresbury Laboratory.[22] In order to minimize the background scattering yield due to the underlying Si crystal matrix, double alignment conditions were employed with the nominally 100 keV He+ beam entering along the [−1−11] channel and the scattered ions being detected along the [111] blocking direction, giving a scattering angle of 70.5°. This scattering configuration was chosen to provide an optimum between scattered yield per bombardment dose, depth, and mass resolution while still resolving peaks as low as C, which is, in practice, the lowest mass detectable with MEIS. The effective near-surface depth resolution for these conditions is better than 0.8 nm, as determined from the slope of the leading edge of the Si peak recorded on a clean Si surface. This quantity deteriorates with depth as it results from a combination of the system energy resolution and straggling. Samples were exposed to a dose of 5 μC per energy-scattering angle (E-Θ) tile (a level determined to be nonperturbing), after which the pass energy of the energy analyzer was adjusted. After completion of the data collection, the individual tiles were merged to form a two-dimensional data set of scattering yield against angle (27°) and energy (60–100 keV), from which cuts were taken along the [111] blocking direction to yield energy spectra of the scattered ions. In order to smooth out any possible tile edge errors, data were collected twice at offset analyzer pass energies and in the case of the nitrided (DPN) samples, four times to ensure a sufficient yield of ions scattered off nitrogen atoms with acceptable statistics.

III. QUANTITATIVE MEIS ANALYSIS AND SIMULATION MODEL DESCRIPTION

The conversion of a MEIS energy spectrum into quantitative depth profiles of the constituent elements contributing to the spectrum relates to two main aspects, i.e., depth and concentration. The conversion of the energy scale into a depth scale relies on an accurate knowledge of the energy dependent inelastic energy loss rates (dE/dx) in the target material. These data are well documented and are obtained from the SRIM code.[23] The procedure is comparatively straightforward for a single species such as a dilute As implant in Si,[8] but becomes substantially more complex in the case of the analysis of multilayers with substantially different energy loss rates in each of the layers. It is most accurately performed by appropriate spectrum simulation as described below. On the other hand, the conversion of scattering yield scale is achieved through an internal calibration by comparing, e.g., the Hf yield with the random Si yield level at the surface, obtained from an amorphized Si sample, after taking into account the squared ratio of the scattering cross sections for Si and Hf, $(Z_1/Z_2)^2$, where Z is the atomic number.[24] This procedure is correct as long as the cross sections for scattering at the energies used are Rutherford-like. However, for typical MEIS energies (100 keV) they are not, as electron screening of the nucleus still occurs and this effectively reduces the cross section for scattering and thus the scattering yield. To account for this deviation, the Andersen correction[25] can be applied. Moreover the effects of the degree of neutralization of the He particle when emerging from the sample surface also reduces the scattered ion yield. An extensive compilation of experimental charged fraction measurements made at the FOM Institute for both H and He (Ref. 26) and results by Kim *et al.*[10] for H indicates that these charged fractions appear to be only dependent on the analyzed energy and agree quite well with the data by Marrion and Young,[27] although Kido *et al.*[28] found deviations.[28] Since in MEIS only charged particles are analyzed, this correction becomes important especially when He ions are used, as in this study. The convolution of these two corrections as a function of the analyzed species can be expressed in a correction curve for the Rutherford cross section ratio between the specific species analyzed (e.g., O or Hf) and the bulk material (Si), normalized for Si. Calculated correction curves for He projectiles at energies of 50, 100, and 200 keV scattered through 70.5° (i.e., [−1−11] in, [111] out) are shown in Fig. 1 as a function of Z. It shows that this correction is both mass and energy dependent, as expected since the energy after scattering depends on the target atomic mass. Neutralization has its strongest effect on the ion yields for scattering off low masses (leading to low energies and a high degree of neutralization) whereas for scattering off higher masses (e.g., Hf), where the interpenetration of the electron clouds during scattering is incomplete, the Andersen correction has the stronger influence. Interestingly, the combined effects of these corrections cancel each other to some degree for atomic masses in the medium range. For the masses analyzed in this study, the combined correction fac-
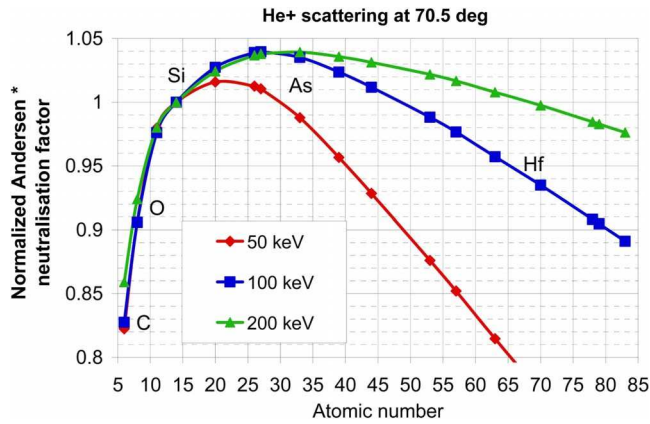
FIG. 1. (Color online) Correction factor to the Rutherford cross section ratio $(Z_1/Z_2)^2$ for He scattering through 70.5° normalized to Si, accounting for the Andersen correction to the scattering cross section and the degree of neutralization of the He projectiles upon emergence from the target.

tors cause reductions in ion yield of ∼7% and 9% for 100 keV He$^+$ scattering off Hf and O, respectively, increasing to ∼13% for N, as compared to the Rutherford cross section ratio. Clearly these corrections need to be taken into account when trying to extract quantitative data from MEIS spectra.

The simulation model used in this work for the quantitative analysis of multilayer/component systems was developed at Daresbury Laboratory[17] as a large macro within the IGOR© graphics software.[16] As a first step, the energy spectrum obtained is fitted with a multipoint curve to subtract the dechanneling background. A sample layer structure based on available information (e.g., film growth parameters or inferred from the peak positions in the MEIS spectrum) is entered together with the scattering geometry parameters, beam energy, and near-surface depth resolution. Energy dependent inelastic energy loss rates as obtained from SRIM (Ref. 23) using best known compound densities are entered as look up tables for different layer compositions (e.g., SiO$_2$ or Hf$_2$O). The assumed layer structure is sliced up in the model into layers of, say, 0.1 nm thick. Each of these slices is transformed into Gaussians with leading and trailing edges that, at the surface, are determined by the depth resolution of the MEIS system. Note that the asymmetric peakshape observed in MEIS for scattering off a monolayer[29,30] is presently not implemented in the program. The degradation of the system resolution with depth is accounted for by introducing an amount of straggling for each layer which results in a reduction in slope of the Gaussians with increasing depth. This dependence is based on measurements of the broadening of multiple Ta delta layers in Si. The Z_2^2 dependence of the cross sections for scattering of the different species present is taken into account to determine the backscattering yield, and the Andersen correction and neutralization corrections are available in the model. The simulation effectively runs through the trial structure summing all the Gaussian contributions to each scattering peak in the spectrum and so determines the overall yield as a function of energy from the assumed input structure. The sum of the relative atomic concentrations of all the species present is normalized at the surface. The simulated energy spectrum (fit) is displayed in comparison with the measured MEIS spectrum. Since several aspects of the MEIS spectrum are only, or predominantly, dependent on one parameter, these are fitted first, (semi)independently. A best structure is arrived at by minimizing the X_{min}^2 value of the overall fit and this value gives an objective reference for the best overall match. In practice, a good visual fit to all the parts of the MEIS spectrum turns out to be a remarkably good measure. Changing the thickness of a layer in the simulation model by 0.1 nm from the best fit result clearly shows a visibly worse match and hence the accuracy of the thickness of layer with a sharp interface can be said to be to be easily better than 0.2 nm. Note that the "depth resolution" definition in the context of determining the error in the layer width differs from that given above, as it is measured between the half heights of the leading and trailing edges of a specific peak caused by a thin layer.

IV. RESULTS AND DISCUSSION

In order to illustrate the changes in the spectra due to changing a growth parameter/process, the results are split into three groups: (i) Si/SiO$_2$ without a Hf layer (to define the starting surface), (ii) added HfO$_2$ layer, and (iii) added HfSiO$_x$ layer. In each case the energy spectrum is displayed (data points) along with the best fit simulated spectrum (line). The depth profiles derived using the simulation model are shown below for each group of samples. The inelastic energy loss rates were calculated by SRIM, assuming densities of 2.3 g/cm^3 for SiO$_2$ and 9.7 g/cm^3 for HfO$_2$. For the Hf silicate layers, the program applies Bragg's rule.

Figure 2 shows the energy spectra of scattered He$^+$ ions (with peaks marked), the best fit simulated spectra, and the resulting depth profiles for samples D02 (Si/SiO$_2$) and D03 (Si/SiO$_2$/DPN). The two spectra were recorded with at least 1 keV different beam energy, causing different peak positions for corresponding peaks. Without "forcing" the surface silicon oxide composition into the model, the resulting structure obtained for the best fit model was a 1.1 nm suboxide with O:Si ratio ≅1 at the surface for both samples. Since the x-ray photoelectron spectroscopy (XPS) measurements of these samples performed within the ANNA project[31] confirm the actual presence of SiO$_2$ at the surface, the model was rerun imposing this composition at the surface. In the composition depth profile, fractional compositions are displayed (the sum of the component fractions is normalized to 1 at the surface). For the forced model, the thickness of the oxide layer is found to be 1.2 nm, as determined by the half height of the decaying flank of the O signal, close to the nominal value of 1 nm. Layer interfaces are broadened by the convolution with the MEIS depth resolution, the straggling, and an adjustable, depth dependent interface slope parameter and would in reality be sharper than shown in the figure. Note that due to the double alignment configuration used, only the top Si atoms and any disordered Si are visible to the beam and this accounts for the decaying Si signal with increasing depth. The effect of DPN in the nitrided sample is clearly
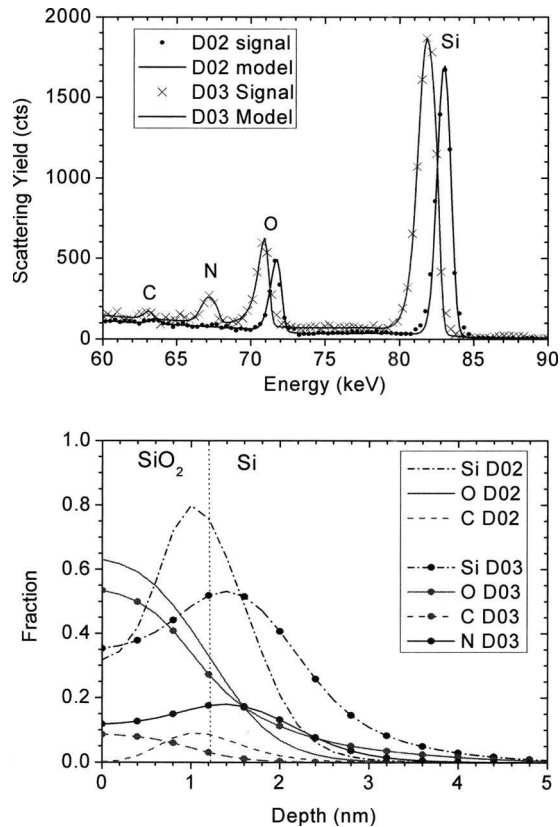
FIG. 2. Energy spectra, model simulations, and depth profiles for layers D02 (Si/SiO_2) and D03 ($Si/SiO_2/DPN$).

FIG. 3. Energy spectra, model simulations, and depth profiles for layers D05 ($Si/SiO_2/HfO_2$) and D06 ($Si/SiO_2/HfO_2/DPN$).

seen in the appearance of the N peak in the spectrum, as marked. The fraction of N in the oxide is measured at the 10%–15% level and increases toward the back of the oxide probably due to leaching of N from the layer caused by re-oxidation, following exposure to air. The presence of N low-ers the O content in the oxide, as shown. DPN also causes Si to be visible to the beam at a greater depth (by ~0.5 nm) and thus it appears that the plasma treatment increases the degree of disorder in the underlying crystalline Si structure. This is a general observation after DPN which is not unexpected as the process involves N bombardment of the surface. It ap-pears that DPN also causes N penetration into the underlying Si, diluting the Si as shown by the reduced Si signal. Finally, the MEIS spectrum suggests the presence of <10% C con-tamination in the surface layer for the nitrided sample D03, as well as some C ($\leq10\%$) at the Si/SiO_2 interface for the sample D02.

The effect of adding a nominally 2 nm HfO_2 layer to the starting layer of D02 and subsequent DPN is shown in the energy spectra and depth profiles in Fig. 3 for samples D05 ($Si/SiO_2/HfO_2$) and D06 ($Si/SiO_2/HfO_2/DPN$). Model simulations indicate that the top layers are stoichiometric HfO_2 and have thicknesses of 1.5 and 1.6 nm for the non-nitrided and the DPN samples, respectively, i.e., 25% and 20% less than the nominal thickness of 2 nm. DPN results in a small N peak in the spectrum representing an ~5% N content in the HfO_2 layer, somewhat increasing into the SiO_2
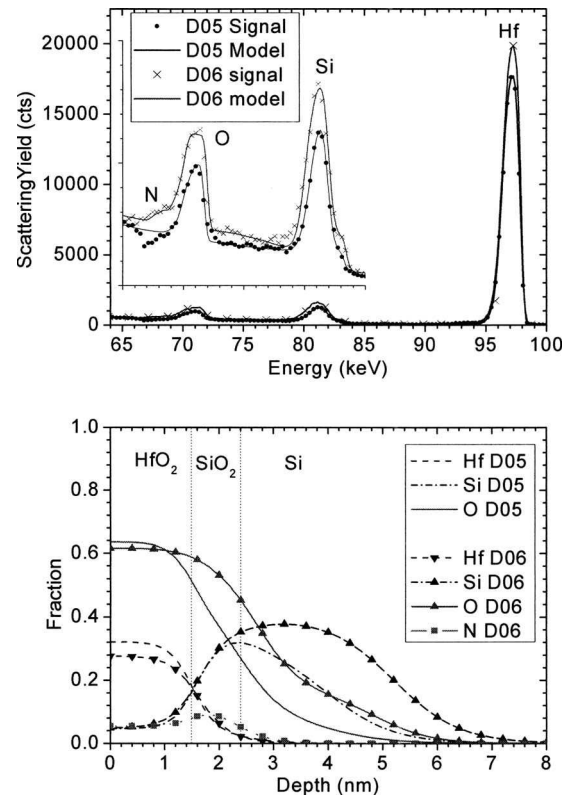
layer and, as expected, a corresponding small reduction in the O content in the oxide layer. Some dilution of the Hf level is also seen. Sample D05 shows an O profile with a decaying flank that extends 0.8–0.9 nm beyond the Hf edge. This gives an estimate for the SiO_2 layer thickness which is again fairly close to the nominal value of 1 nm. Similar to sample D03, the greater depth of the Si profile post-DPN in Fig. 3 shows that the treatment causes an increase in depth of the Si lattice disorder and some drive-in of the oxygen. In-terestingly, MEIS shows the presence of 5%–6% Si in the Hf layer, as is seen in the high energy shoulder on the Si peak at ~83 keV. The cause of this is not clear but it may be due to a reaction of HfO_2 with Si during growth or possibly the presence of pores in the ultrathin layers. XTEM of these samples show that the HfO_2 layers are recrystallized and that layer interfaces are comparatively rough.[32]

In the series shown in Fig. 4, the HfO_2 layer of samples D05 and D06 was replaced by a nominally 2 nm Hf silicate yielding samples D07 $[Si/SiO_2/HfSiO_x(60\%Hf)]$ and D08 $[Si/SiO_2/HfSiO_x(60\%Hf)/DPN]$. In sample D09, an addi-tional DPN of the underlying SiO_2 was added ($Si/SiO_2/DPN/HfSiO_2$ (60%Hf)/DPN). The changes in the MEIS spectra and simulated depth profiles are clearly vis-ible. In the Hf silicate samples, the Hf contents are found to be 58.5% and 62%, i.e., within 2% of the nominal 60% value. In this case, too, the layer thicknesses are measured to be well below the nominal value of 2 nm, at 1.4 nm for D07 and D08 and at 1.5 nm for D09. As for samples D05 and
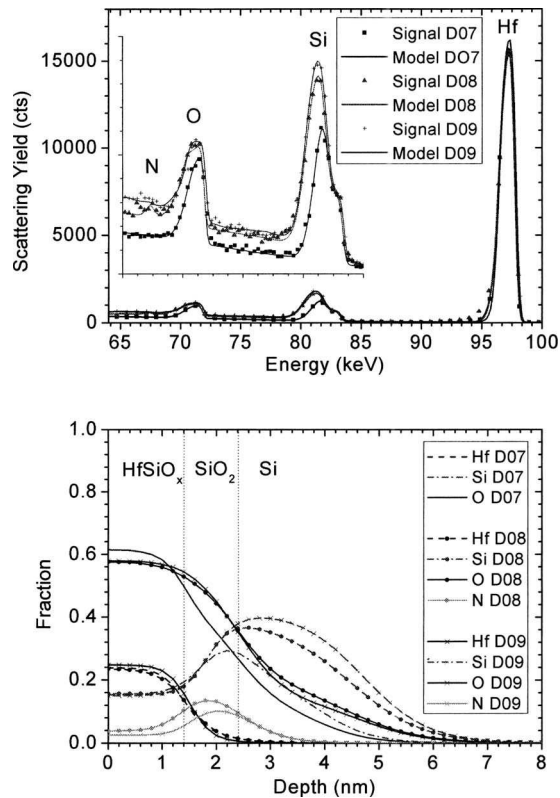
FIG. 4. Energy spectra, model simulations, and depth profiles for layers D07 [Si/SiO$_2$/HfSiO$_x$ (60%Hf)], D08 [Si/SiO$_2$/HfSiO$_x$ (60%Hf)/DPN], and D09 [Si/SiO$_2$/DPN/HfSiO$_x$ (60%Hf)/DPN].

D06, the thickness of the buried SiO$_2$ layer is more difficult to determine accurately, but based on the depths of the half heights of the O profiles, they are estimated at between 0.8 and 1.0 nm. For layer D08, DPN is observed to lead to a 4% N content in the Hf silicate layer rising to 10% at the back of this layer, a finding that, as above, is attributed to oxidation near the surface. Layer D09 appears to have almost no N near the surface, but a N level similar to D08 near the silicate interface. Finally, as above, DPN drives in the O profile and increases the depth of Si disorder.

Studies of these samples performed within the ANNA project with alternative techniques were used for cross comparison of the measurements of the layer thicknesses. A XTEM micrograph of sample D07 is shown in Fig. 5.[32] Unlike as seen in the HfO$_2$ layers (D05, D06), there is no evidence of the presence of crystalline grains in the Hf silicate. The layers show a pronounced surface roughness which is
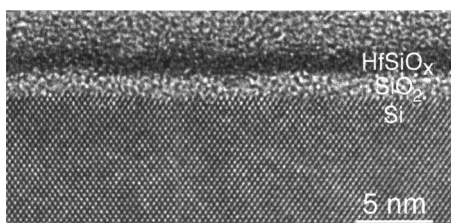

FIG. 5. Cross-sectional high resolution electron microscopy (HREM) micrograph of sample D07 [Si/SiO$_2$/HfSiO$_x$ (60%Hf)].

strongly reduced after DPN treatment. The HfSiO$_x$ layer thickness determined for this layer is 1.3 ± 0.1 nm which compares well to the MEIS result of 1.4 nm. Note that the area of ion beam spot in MEIS is typically of the order of 0.1 mm^2, many orders of magnitude larger than XTEM, and hence any interface roughness seen in XTEM would result in profile broadening in MEIS. Absolute, reference-free x-ray fluorescence (XRF) measurements of this sample yield again a thickness of 1.4 nm $\pm$ 20%,[33] but angle dependent XPS data give a somewhat higher value of 1.9 ± 0.2 nm.[31] Taken together these results represent a good overall convergence of the measurements.

Finally, the experience gained from the optimization of the spectrum simulation program afforded by the analysis of the sample series discussed above, in conjunction with optimum MEIS analysis conditions has been applied in the analysis by MEIS of a more complex, ~7 nm wide, high-k, metal gate stack with the following nominal structure: TiN(3 nm)/Al$_2$O$_3$(0.9 nm)/HfO$_2$(2 nm)/SiO$_2$(1 nm)/Si. The thin Al$_2$O$_3$ layer was inserted in the stack to obtain a suitable modification of the workfunction of the metal gate,[18] which could be due to a compositional modification of the interface. Depth profile analysis of the constituents may shed light on the process. Samples were analyzed before (D13) and after (D14) annealing to 1025 °C for 1 min in an inert gas atmosphere. Containing five layers and six elements, this structure represents a challenging problem for MEIS as well as the simulation model which at present can only process four different elements simultaneously. This limitation was accommodated by ignoring the presence of the underlying SiO$_2$/Si layers in the simulation. Energy spectra with the various peak origins annotated, based on the energies at which they occur, together with best fit sample structures before and after annealing, are shown in Fig. 6. The simulated film structure before annealing reproduces the as grown film layer parameters with good accuracy as indicated in the profile graph: 3 nm TiN (surface oxidized), 0.9 nm AlO$_x$, and 1.7 nm HfO$_2$. The most significant observation is that after annealing the Hf peak has shifted by about 1 keV toward higher energy which in the depth profiles is reflected as a shift of the Hf profile by ~0.4 nm toward the surface, i.e., a move of Hf into the AlO$_x$ caplayer. Note that the back edge of the TiN layer remains unchanged (only postannealing Ti and N profiles are shown for clarity). The movement of Hf implies a reverse Al diffusion into the Hf oxide layer and this is indeed seen in the simulation in the Al profile which as a result has reduced in height. This is in agreement with TOF-SIMS results[18] and suggests compositional changes at the interface may be associated with the observed workfunction change. There is no MEIS evidence for Al diffusion into the TiN layer, as seen by time-of-flight secondary ion mass spectrometry (TOFSIMS).[18] The postannealing MEIS spectrum finally shows that this treatment results in an ~1% Hf segregation at the surface as indicated by the surface Hf marker.

V. CONCLUSION

Multilayer nanofilms of SiO$_2$, HfO$_2$, and HfSiO$_x$ down to $1-2$ nm thickness, before and after plasma nitridation, were
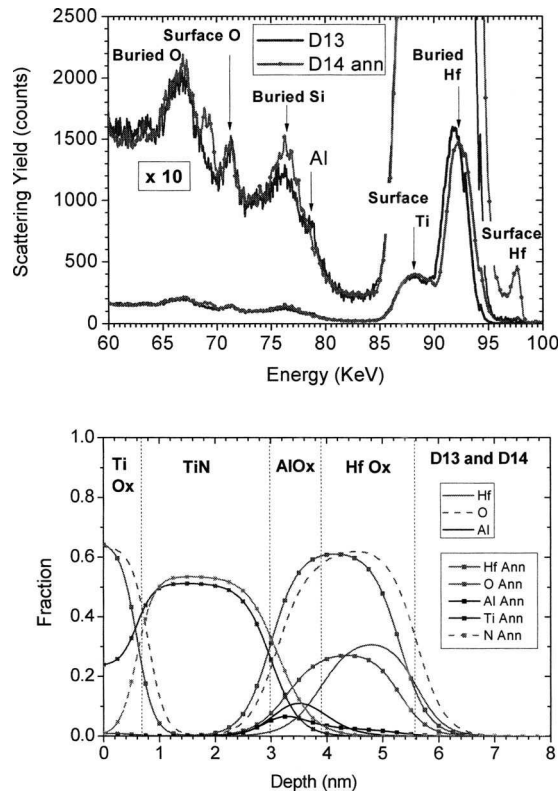
FIG. 6. MEIS energy spectra and derived depth profiles of a nominal TiN(3 nm)/Al$_2$O$_3$(0.9 nm)/HfO$_2$(2 nm)/SiO$_2$(1 nm)/Si metal gate high-*k* stack, showing Hf and Al interdiffusion, postannealing.

analyzed by MEIS experiments in conjunction with a spectrum simulation model[17] that takes proper account of all the collisional effects such as composition dependent stopping, straggling, and includes neutralization and cross section corrections. The degree of yield correction required to the straightforward application of the Rutherford cross section is graphically illustrated as a function of atomic number of the target species. Results demonstrate the capability of MEIS to provide high depth resolution, quantitative compositional, and structural analysis on high-*k* nanofilms. Film thickness was determined to an accuracy of ±0.1 nm and the stoichiometry of the layers was found to be well within a few percent of the nominal as grown parameters. The results were cross referenced to measurements from absolute, reference-free XTEM, XRF, and XPS and good overall agreement was found, which strengthens confidence in the model simulations. DPN was shown to cause recoil implantation of O into the underlying Si and an increase in depth of the disorder in the Si lattice. MEIS was next applied to characterization of a complex high-*k*, metal gate structure. Not only did it closely confirm the as grown film parameters, but significantly, it showed the diffusion, after thermal treatment at 1025 °C, of Hf into the Al caplayer inserted to adjust the metal gate workfunction, probably through chemical modification of the interface,[18] and vice versa.

[1]D. Schlom, S. Guha, and S. Datta, MRS Bull. **33**, 1017 (2008).
[2]http://www.intel.com/technology/architecture-silicon/45nm-core2/.
[3]C. S. Kang, R. Choi, H. J. Cho, Y. H. Kim, and J. C. Lee, J. Vac. Sci. Technol. B **22**, 916 (2004).
[4]H. Kobayashi, K. Imamura, K. Fukayama, S. Im, O. Maida, Y. Kim, H. Kim, and D. Choi, Surf. Sci. **602**, 1948 (2008).
[5]http://www.i3-anna.org/.
[6]T. Gustafsson, H. C. Lu, B. W. Busch, W. H. Schulte, and E. Garfunkel, Nucl. Instrum. Methods Phys. Res. B **183**, 146 (2001).
[7]J. A. van den Berg, G. Carter, D. G. Armour, M. Werner, R. D. Goldberg, E. H. J. Collart, P. Bailey, and T. C. Q. Noakes, Appl. Phys. Lett. **85**, 3074 (2004).
[8]M. Werner, J. A. van den Berg, D. G. Armour, W. Vandervorst, E. H. J. Collart, R. D. Goldberg, P. Bailey, and T. C. Q. Noakes, Nucl. Instrum. Methods Phys. Res. B **216**, 67 (2004).
[9]E. P. Gusev, C. Cabral, M. Copel, C. D'Emic, and M. Gribelyuk, Microelectron. Eng. **69**, 145 (2003).
[10]J. Kim, W. N. Lennard, C. P. McNorgan, J. Hendriks, I. V. Mitchell, D. Landheer, and J. Gredley, Curr. Appl. Phys. **3**, 75 (2003).
[11]H. S. Chang, H. Hwang, M.-H. Cho, and D. W. Moon, Appl. Phys. Lett. **86**, 031906 (2005).
[12]K. B. Chung, C. N. Whang, H. S. Chang, D. W. Moon, and M.-H. Cho, J. Vac. Sci. Technol. A **25**, 141 (2007).
[13]H. Kitano, S. Abo, M. Mizutani, J. Tsuchimoto, T. Lohner, J. Gyulai, F. Wakaya, and M. Takai, Nucl. Instrum. Methods Phys. Res. B **249**, 246 (2006).
[14]S. Bernardini, M. MacKenzie, O. Buiu, P. Bailey, T. C. Q. Noakes, W. M. Davey, B. Hamilton, and S. Hall, Thin Solid Films **517**, 459 (2008).
[15]L. Miotti, R. P. Pezzi, M. Copel, and I. J. R. Baumvol, Nucl. Instrum. Methods Phys. Res. B **266**, 1162 (2008).
[16]IGOR PRO, Wavemetrics (http://www.wavemetrics.com).
[17]P. Bailey *et al.* (unpublished).
[18]T. Conard, A. Franquet, W. Vandervorst, M. Reading, J. A. Van den Berg, S. Van Elschocht, T. Schram, and S. Degendt, ECS Trans. **16**, 433 (2008).
[19]F. De Smedt, C. Vinckier, I. Cornelissen, S. Degendt, and M. Heyns, J. Electrochem. Soc. **147**, 1124 (2000).
[20]C. H. Cheng *et al.*, IEEE Electron Device Lett. **22**, 378 (2001).
[21]S. F. Jang *et al.*, IEEE Electron Device Lett. **22**, 327 (2001).
[22]P. Bailey, T. C. Q. Noakes, and D. P. Woodruff, Surf. Sci. **426**, 358 (1999). (http://www.dl.ac.uk/MEIS/).
[23]J. F. Ziegler, SRIM code (http://www.srim.org/).
[24]W. K. Chu, J. W. Mayer, and M. Nicolet, *Backscattering Spectrometry* (Academic, New York, 1978).
[25]H. H. Andersen, F. Besenbacher, P. Loftager, and W. Moeller, Phys. Rev. A **21**, 1891 (1980).
[26]P. Bailey (private communication).
[27]J. B. Marrion and F. C. Young, *Nuclear Reaction Analysis: Graphs and Tables* (North-Holland, Amsterdam, 1968).
[28]Y. Kido, T. Nishimura, Y. Hoshino, E. Toyoda, and T. Nakada, Phys. Rev. B **64**, 193403 (2001).
[29]P. L. Grande, A. Hentz, R. P. Pezzi, I. J. R. Baumvol, and G. Schiwietz, Nucl. Instrum. Methods Phys. Res. B **256**, 92 (2007).
[30]R. P. Pezzi, P. L. Grande, M. Copel, G. Schiwietz, C. Krug, and I. J. R. Baumvol, Surf. Sci. **601**, 5559 (2007).
[31]S. Ladas *et al.* (unpublished).
[32]A. Parisini *et al.* (unpublished).
[33]M. Kolbe, B. Beckhoff, M. Krumrey, M. Reading, J. Van den Berg, T. Conard, and S. De Gendt, ECS Trans. **25**, 293 (2009).